Cell Reports
Methods

Article

A Flp-dependent G-CaMP9a transgenic mouse for neuronal imaging *in vivo*

Graphical abstract

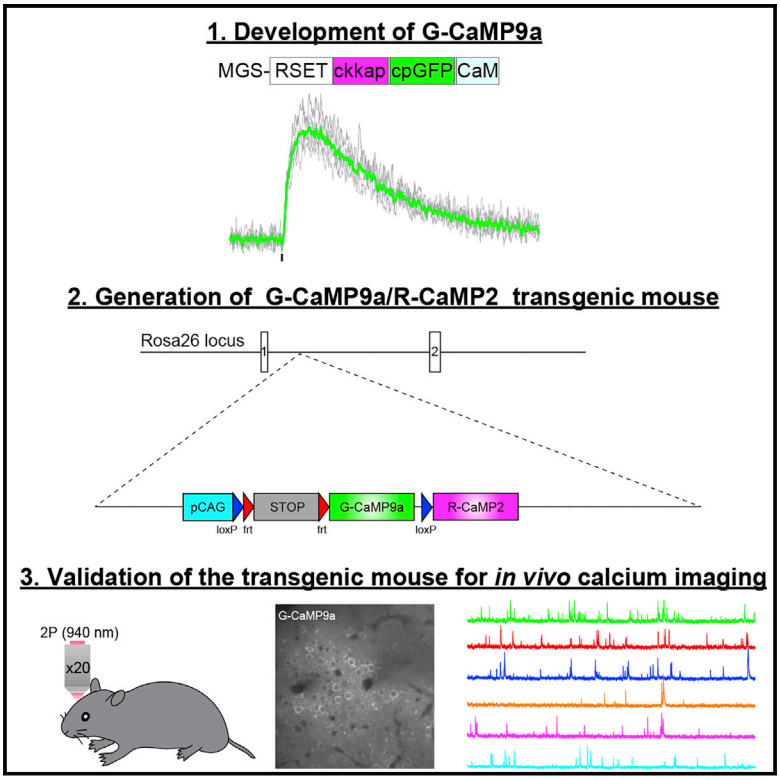

Highlights

- Develops a fast and high signal-to-noise ratio GECI, G-CaMP9a
- Generates a Rosa26 knockin mouse expressing G-CaMP9a in a Flp-dependent manner
- Spontaneous and sensory-evoked neuronal activities are measured
- Coexpressing red GECI enables versatile dual-color imaging

Authors

Masayuki Sakamoto, Masatoshi Inoue, Atsuya Takeuchi, ..., Kazuo Kitamura, Hajime Fujii, Haruhiko Bito

Correspondence

sakamoto.masayuki.2e@kyoto-u.ac.jp (M.S.),
hbito@m.u-tokyo.ac.jp (H.B.)

In brief

Sakamoto et al. generate and validate a Rosa26 knockin mouse transgenic line called G-CaMP9a that is driven by a ubiquitous CAG promoter. The reporter line expresses a genetically encoded calcium indicator with a fast and high signal-to-noise ratio in a Flp-recombinase-dependent manner.

Sakamoto et al., 2022, Cell Reports Methods *2*, 100168
February 28, 2022
https://doi.org/10.1016/j.crmeth.2022.100168

CellPress

Cell Reports Methods

CellPress
OPEN ACCESS

Article

A Flp-dependent G-CaMP9a transgenic mouse for neuronal imaging *in vivo*

Masayuki Sakamoto,[1,2,3,12,*] Masatoshi Inoue,[1,4,12] Atsuya Takeuchi,[5,11] Shigetaka Kobari,[1] Tatsushi Yokoyama,[1,2] Shin-ichiro Horigane,[1,6,7] Sayaka Takemoto-Kimura,[1,3,6,7] Manabu Abe,[8] Kenji Sakimura,[8] Masanobu Kano,[5,9] Kazuo Kitamura,[5,10] Hajime Fujii,[1] and Haruhiko Bito[1,9,13,*]

[1]Department of Neurochemistry, Graduate School of Medicine, The University of Tokyo, Hongo7-3-1, Bunkyo-ku, Tokyo 113-0033, Japan
[2]Department of Optical Neural and Molecular Physiology, Graduate School of Biostudies, Kyoto University, Kyoto 606-8507, Japan
[3]Precursory Research for Embryonic Science and Technology (PRESTO), Japan Science and Technology Agency, Kyoto 606-8507, Japan
[4]Department of Bioengineering, Stanford University, Stanford, CA 94305, USA
[5]Department of Neurophysiology, Graduate School of Medicine, The University of Tokyo, Bunkyo-ku, Tokyo 113-0033, Japan
[6]Department of Neuroscience I, Research Institute of Environmental Medicine, Nagoya University, Nagoya, Aichi 464-8602, Japan
[7]Department of Molecular/Cellular Neuroscience, Nagoya University Graduate School of Medicine, Nagoya, Aichi 466-8550, Japan
[8]Department of Animal Model Development, Brain Research Institute, Niigata University, Niigata 951-8585, Japan
[9]International Research Center for Neurointelligence (WPI-IRCN), The University of Tokyo, Bunkyo-ku, Tokyo 113-0033, Japan
[10]Department of Neurophysiology, Faculty of Medicine, University of Yamanashi, Chuo, Yamanashi 409-3898, Japan
[11]Department of Neurophysiology, School of Dentistry, Tokyo Medical and Dental University, Tokyo, Japan
[12]These authors contributed equally
[13]Lead contact
*Correspondence: sakamoto.masayuki.2e@kyoto-u.ac.jp (M.S.), hbito@m.u-tokyo.ac.jp (H.B.)
https://doi.org/10.1016/j.crmeth.2022.100168

MOTIVATION To date, a variety of transgenic mouse lines producing robust genetically encoded calcium indicator (GECIs) expressions in selected neurons have been generated. However, some GECI-expressing mouse lines have shown significant abnormalities in their brain. To overcome these issues, we generate and characterize a Rosa26 knockin mouse line called G-CaMP9a that is driven by a strong CAG promoter and expresses a green GECI with fast kinetics and a high signal-to-noise ratio in a Flp-dependent manner. This reporter allows for the investigation of neuronal activity in defined populations *in vivo* and will facilitate dissecting complex dynamics of neural networks *in vivo*.

SUMMARY

Genetically encoded calcium indicators (GECIs) are widely used to measure calcium transients in neuronal somata and processes, and their use enables the determination of action potential temporal series in a large population of neurons. Here, we generate a transgenic mouse line expressing a highly sensitive green GECI, G-CaMP9a, in a Flp-dependent manner in excitatory and inhibitory neuronal subpopulations downstream of a strong CAG promoter. Combining this reporter mouse with viral or mouse genetic Flp delivery methods produces a robust and stable G-CaMP9a expression in defined neuronal populations without detectable detrimental effects. *In vivo* two-photon imaging reveals spontaneous and sensory-evoked calcium transients in excitatory and inhibitory ensembles with cellular resolution. Our results show that this reporter line allows long-term, cell-type-specific investigation of neuronal activity with enhanced resolution in defined populations and facilitates dissecting complex dynamics of neural networks *in vivo*.

INTRODUCTION

Measuring the dynamics of neural circuits at high spatial-temporal resolutions is crucial for deciphering complex interactions between distributed neuronal populations that work together to generate internal brain states and behavior. To do this, it is necessary to measure neural activity in multiple sets of neuronal subpopulations accurately. The activity of large numbers of neurons can be monitored through optical methods. Because action potentials (APs) generated at axon hillocks necessarily trigger calcium influxes in the cell soma, calcium imaging is widely used as a reliable and quantitative readout for monitoring neural activity in multiple neurons simultaneously (Ahrens et al., 2013; Cossart et al., 2003; Kato et al., 2012; Komiyama et al., 2010). Recent technical advances in two-photon microscopy allow for the measurement of spiking activity from hundreds to thousands

of neurons in neural circuits with a cellular resolution during behavior *in vivo* (Dombeck et al., 2010; Huber et al., 2012; Ota et al., 2021; Peters et al., 2014; Sofroniew et al., 2016; Stirman et al., 2016). In parallel, a variety of genetically encoded calcium indicators (GECIs) with a high signal-to-noise ratio (SNR) and fast kinetics have been developed (Chen et al., 2013; Dana et al., 2016, 2019; Inoue et al., 2015, 2019; Nakai et al., 2001; Ohkura et al., 2012; Zhao et al., 2011), making it possible to tease apart complex dynamics of brain activities at the cellular level.

Despite the progress in the performance and application of GECIs, however, several challenges remain. Quantitative GECI imaging *in vivo* requires high-level expressions in determined cell populations. Such high expression levels can be obtained by gene-transfer techniques, such as *in utero* electroporation and adeno-associated virus (AAV) infection, resulting in high transgene copy numbers in individual neurons (Chen et al., 2013; Dana et al., 2016; Tian et al., 2009). Although these approaches are powerful, there are still some drawbacks, such as invasive surgery, uneven gene expression across cell populations, and incomplete coverage in given targeted populations (Chen et al., 2013; Tian et al., 2009). Because the copy number of transfected virus vectors or electroporated plasmids is variable among neurons, amplitudes and kinetics of calcium transients may vary significantly among the targeted population, thus obscuring the clarity of the quantification. Furthermore, cytotoxicity might arise due to uncontrolled gene expression and/or long-term virus infection (Chen et al., 2013; Zariwala et al., 2012). Moreover, the leak of the virus or plasmid outside of the injection or electroporated sites is a general concern that may reduce regional specificity.

Transgenic methods could potentially solve these issues. If driven from a single locus in limited copy number, transgenic expression can be stable within an area, with slight cell-to-cell variance, and persist over an animal's entire lifetime (Direnberger et al., 2012; Zariwala et al., 2012). Also, expression patterns and levels are reproducible across different individual animals. To date, a variety of transgenic mouse lines producing robust GECI expression in selected neurons have been generated (Bethge et al., 2017; Chen et al., 2012; Daigle et al., 2018; Dana et al., 2014, 2018; Direnberger et al., 2012; Madisen et al., 2015; Sato et al., 2015; Wekselblatt et al., 2016; Zariwala et al., 2012), demonstrating the advantages of transgenic control of GECI expression. For instance, Thy1 promoter transgenic mice reliably achieve high-level expressions by chromosomal integration of GECI transgenes with multiple copies. However, although it is powerful, the expression of transgene driven by the Thy1 promoter is strongly position-dependent, necessitating a screening of multiple founder lines to identify potentially useful lines. Also, the Thy1 promoter drives expression mostly in pyramidal neurons and scarcely targets GABAergic interneurons. Recently, a new Cre- and tetracycline transactivator (tTA)-dependent transgenic platform (TIGRE) was developed, achieving a higher gene expression than Rosa26-based lines (Daigle et al., 2018; Madisen et al., 2015). However, some GECI-expressing, TIGRE-based mouse lines were reported to show significant abnormalities in their brain activity (Daigle et al., 2018; Steinmetz et al., 2017). Also, tTA is a potent transcriptional transactivator that may cause neurodegeneration when expressed at high levels (Han et al., 2012).

To overcome these issues, we generated and characterized a Rosa26 knockin mouse line that expresses a green GECI with fast kinetics and a high SNR, named G-CaMP9a, in a Flp-dependent manner driven by a strong CAG promoter. Combining this reporter mouse with appropriate Flp delivery methods (Flp-expressing transgenic mice, AAV, or *in utero* electroporation) produced robust and stable G-CaMP9a expression in defined neuronal populations in the cortex. Using this transgenic mouse, we could detect spontaneous and sensory-evoked calcium transients in excitatory and inhibitory neurons at single-cell resolution with two-photon microscopy. Our results show that this reporter line allows for the investigation of neuronal activity in defined populations *in vivo* and will notably facilitate dissecting complex dynamics of neural networks *in vivo*.

RESULTS

Generation of an interleaved G-CaMP9a knockin mouse

Using a strategy employed previously (Inoue et al., 2015), we developed a green, fast, and high SNR GECI, named G-CaMP9a, by replacing the Ca^{2+}/calmodulin (CaM)-binding domain peptide sequence (based on muscle myosin light chain kinase) of G-CaMP 4.1 with ckkap (a peptide sequence responsible for binding Ca^{2+}-bound CaM within the primary structure of CaMKK-α) (Figure 1A) (Shindo et al., 2010). Compared with GCaMP6f and GCaMP6s, G-CaMP9a had higher calcium binding affinities and lower Hill coefficients (Table 1). We then tested the performance of the GECI in acute brain slices of layer 2/3 barrel cortex pyramidal neurons. Mouse embryos at embryonic day 14.5 were *in-utero*-electroporated with pTREtight-GCaMP6f, pTREtight-GCaMP6s, or pTREtight-G-CaMP9a plasmids together with pCAG-TetOn3G plasmid. To express GECIs, mice were given water containing doxycycline 5–7 days before the experiment. Spike-induced calcium transients were assessed by high-speed (774 Hz), line-scan, two-photon imaging under a whole-cell patch-clamp configuration (Figures 1B–1G; Table S1). While the $\Delta F/F$ response to a single AP was unchanged (Figure 1B), G-CaMP9a showed a performance comparable to GCaMP6f and superior to GCaMP6s in terms of rise and decay kinetics (Figures 1F and 1G) and demonstrated an improved SNR in response to single APs compared with both GCaMP6f and GCaMP6s (Figure 1D). Consistent with these enhanced parameters, successive pulses of current injections up to 8 pulses demonstrated that improved $\Delta F/F$ amplitude, SNRs, and decay times, such that we resolved cumulative steps of calcium transients generated by successive pulses of AP trains even with a single trial up to 20 Hz (Figures 1H–1K and S1).

Next, we attempted to design a conditionally expressing G-CaMP9a/R-CaMP2 mouse line (Figure 2A). In this line, the conditional alleles of G-CaMP9a (expressed by Flp-mediated deletion of a STOP cassette) and R-CaMP2 (expressed by a Cre-mediated deletion of a STOP cassette) were knocked in, in a single cassette, at the Rosa26 locus. As Rosa26 is transcriptionally active in almost all tissues, this strategy avoids potential problems associated with a sizable multicopy array and the silencing effects of local chromatin structures that are often observed with randomly integrated transgenic constructs (Imayoshi et al., 2012; Madisen et al., 2010; Soriano, 1999). Recently, in addition

CellPress
OPEN ACCESS

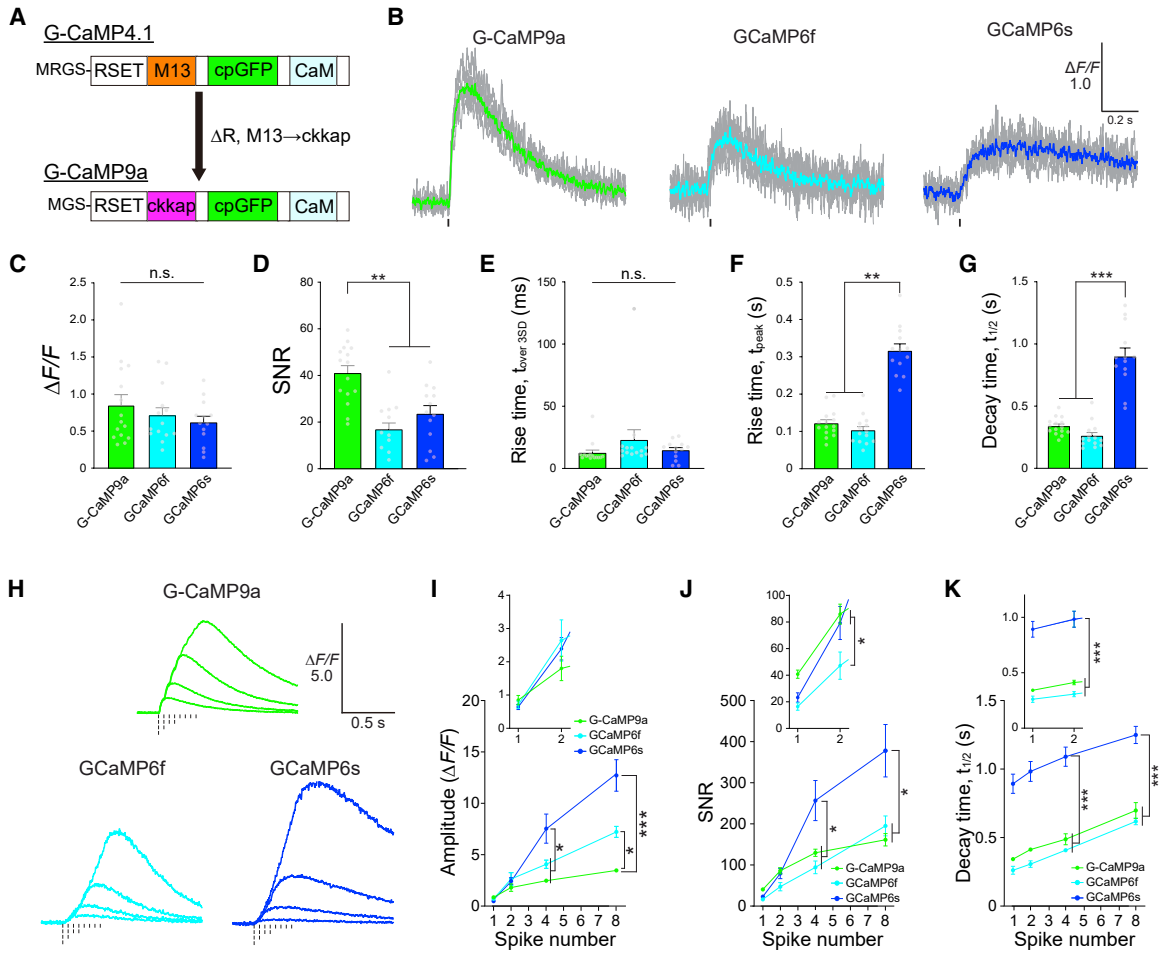

Figure 1. Performance of G-CaMP9a in acute brain slices

(A) Schematic of G-CaMP4.1 and G-CaMP9a.

(B) Representative traces of G-CaMP9a, GCaMP6f, and GCaMP6s fluorescence changes (Δ*F*/*F*) in response to a single AP of the barrel cortex layer 2/3 pyramidal neurons in acute brain slices. The eight-trial average response of a single sweep (gray) and the averages of 8 sweeps (colored) are overlaid. The black vertical lines indicate stimuli.

(C–G) Comparison of G-CaMP9a (n = 15), GCaMP6f (n = 13), and GCaMP6s (n = 14) signals during single AP-triggered somatic calcium transients in an acute cortical slice. Amplitude (Δ*F*/*F*, C, and SNR, D), rise time (first exceeded 3SD time point, E, and time to peak, F), and decay time constants (G) of somatic calcium transients by a single AP. n.s., not significant, **p < 0.01, ***p < 0.001 in Wilcoxon rank-sum test. Error bars represent SEM.

(H) Representative traces of fluorescence response (Δ*F*/*F*) of G-CaMP9a (green), GCaMP6f (cyan), and GCaMP6s (blue) in response to one, two, four, and eight spike trains at 20 Hz.

(I–K) Mean amplitude (I), SNR (J), and decay time constants (K) of G-CaMP9a (n = 14), GCaMP6f (n = 12), and GCaMP6s (n = 12) in response to one to eight spike trains at 20 Hz. Insets represent a magnified view of 1–2 spikes. *p < 0.05, ***p < 0.001 in Tukey's test. Error bars represent SEM.

to the Cre/loxP system, the Flp/Frt recombination system has been widely applied, and a large number of Flp driver transgenic lines are available (Daigle et al., 2018; He et al., 2016; Madisen et al., 2015; Miyoshi et al., 2010; Sakamoto et al., 2014).

We tested whether by removing the frt- or loxP-flanked STOP cassette sequences G-CaMP9a or R-CaMP2 would be expressed under the control of the CAG promoter (a combination of the chicken beta-actin promoter and the cytomegalovirus immediate-early enhancer) (Figure 2B). We injected an AAV encoding Cre (AAV2/1-pCaMKII-iCre-T2A-EGFP) or Flp (AAV2/1-pCAG-Flpo-T2A-TurboFP635) in the barrel cortex and performed immunohistological analyses. We found that AAV-Flp injection triggered the expression of G-CaMP9a in neurons around the injection site (Figure 2C, top panels). However, though AAV-Cre injection led to a successful expression of the recombinase reporter construct, R-CaMP2 expression was extremely weak (Figure 2C, bottom panels), resulting in fluorescence signals that were too dim to monitor neural activity by either one- or two-photon imaging *in vivo*. Therefore, in this study, we solely focused on the validation of the Flp-dependent expression of G-CaMP9a. In line with the result of G-CaMP9a being expressed by *in utero* electroporation (Figure 1), simultaneous electrical recording and optical imaging revealed that the performance of G-CaMP9a in the knockin mice could detect

Table 1. *In vitro* characteristics of G-CaMP9a and GCaMP6

GECI	Ca^{2+}	I_{abs}[a] (ε[b])	I_{em}[c] (QY[d])	Brightness[e]	pKa	Kd (nM)	Hill coefficient
G-CaMP9a	–	401 (69,200) 489 (7,180)	514 (0.11)	0.80	8.70 ± 0.18	59 ± 7	1.6 ± 0.3
	+	395 (7,180) 487 (26,080)	514 (0.45)	11.7	7.69 ± 0.02		
GCaMP6f	–	398 (34,400) 502 (7,600)	514 (0.11)	0.80	6.29 ± 0.03	287 ± 13	3.1 ± 0.4
	+	447 (20,200) 495 (53,900)	514 (0.61)	32.8	9.17 ± 0.24		
GCaMP6s	–	397 (28,800) 508 (2,400)	514 (0.11[f])	0.80	–	153 ± 2	2.7 ± 0.1
	+	447 (16,300) 495 (56,300)	514 (0.61[f])	34.4	–		

[a]Absorbance peak (nm).
[b]Extinction coefficient (M^{-1}/cm^{-1}).
[c]Emission peak (nm).
[d]Quantum yield.
[e]Product of ε and Φ.
[f]Reference: Chen et al. (2013).

single APs in pyramidal neurons in acute brain slices of the layer 2/3 barrel cortex (Figures 2D–2I; Table S1).

Imaging sensory-evoked activity in the visual cortex

We investigated whether a G-CaMP9a knockin mouse can be used to study sensory-evoked cortical activity at single-cell resolution. First, we performed calcium imaging in layer 2/3 pyramidal neurons of the primary visual cortex (V1) of the knockin mice *in vivo*. The majority of V1 neurons can generate APs in response to drifting gratings (Ayzenshtat et al., 2016; Mrsic-Flogel et al., 2007; Niell and Stryker, 2008). To generate G-CaMP9a expression in the knockin mouse, we injected an AAV encoding Flp recombinase under the human synapsin promoter (AAV2/1-phSyn-Flpo) to the V1 at the age of 4 weeks (Figure 3A). Four weeks after virus infection, strong G-CaMP9a fluorescence of layer 2/3 pyramidal neurons was observed by *in vivo* two-photon imaging (Figure 3B). Then, we examined G-CaMP9a-based properties of orientation selectivity in layer 2/3 of V1. Awake head-fixed mice were presented with oriented gratings moving in eight different directions to the contralateral eye. *In vivo* calcium imaging demonstrated that visual stimuli-evoked fluorescence transients were observed in subsets of neurons (Figure 3C; Video S1). These responses were stable across trials and tuned to stimulus orientation. Quantitative analysis revealed that fractions of cells detected as responsive neurons and the orientation selectivity index in the knockin mice were indistinguishable between the G-CaMP9a knockin mice, the G-CaMP9a AAV-injected mice, and the GCaMP6f AAV-injected mice (Figures 3D and 3E), though response amplitudes of G-CaMP9a were significantly lower than those of GCaMP6f (Figure 3F). This result is in keeping with fast kinetics and better linearity of G-CaMP9a. These results suggest that G-CaMP9a-expressing V1 neurons of the knockin mice reveal properties that are similar to those previously identified via *in vivo* electrophysiology (Niell and Stryker, 2008) and other calcium indicators (Chen et al., 2013). Also, this is the first report of a Flp-dependent transgenic line that can monitor neural activity faithfully with cellular resolution.

Imaging activity in the barrel cortex *in vivo*

Next, we conducted *in vivo* two-photon calcium imaging in layer 2/3 pyramidal neurons of the barrel cortex. To induce G-CaMP9a expression, we electroporated a plasmid encoding Flp recombinase under the control of a CAG promoter in heterozygote knockin mouse embryos at embryonic day 15.5 (E15.5) (Figure 4A). The Flp recombination led to efficient homogeneous G-CaMP9a expression in layer 2/3 pyramidal neurons (150–200 μm from the pial surface) of the barrel cortex around the electroporation site (Figure 4B). Then, to examine whether G-CaMP9a could be used to detect sensory-evoked cortical activity with single-cell resolution, we performed *in vivo* two-photon imaging of whisker-deflection-induced responses in the barrel cortex of awake mice between 1 and 5 months of age (Figure 4C). Consistent with previous studies, a small subset of neurons showed robust sensory-evoked calcium transients (Figures 4D and 4E) (Inoue et al., 2015; Inoue et al., 2019; O'Connor et al., 2010; Tada et al., 2014). We also performed *in utero* electroporation at E12.5 to target layer 5 pyramidal neurons (500 μm from the pial surface) in the barrel cortex. Again, this reporter mouse can reliably record spontaneous calcium transients (Figure S2). Moreover, high-speed *in vivo* imaging with a resonant scanner (frame rate: 30 Hz) also acquired spontaneous neuronal activity (Figure S3; Video S2).

Previous studies suggested that long-term expression of GECI introduced by *in utero* electroporation or viral infection may cause altered physiology and sensor properties with strong nuclear fluorescence (Chen et al., 2013; Dana et al., 2016; Tian et al., 2009). To test cell-toxicity effects, we examined *in vivo* two-photon calcium imaging in layer 2/3 pyramidal neurons of the barrel cortex at 5 months of age (continuous expression for 5 months). Again, G-CaMP9a detected sensory-evoked cortical

CellPress
OPEN ACCESS

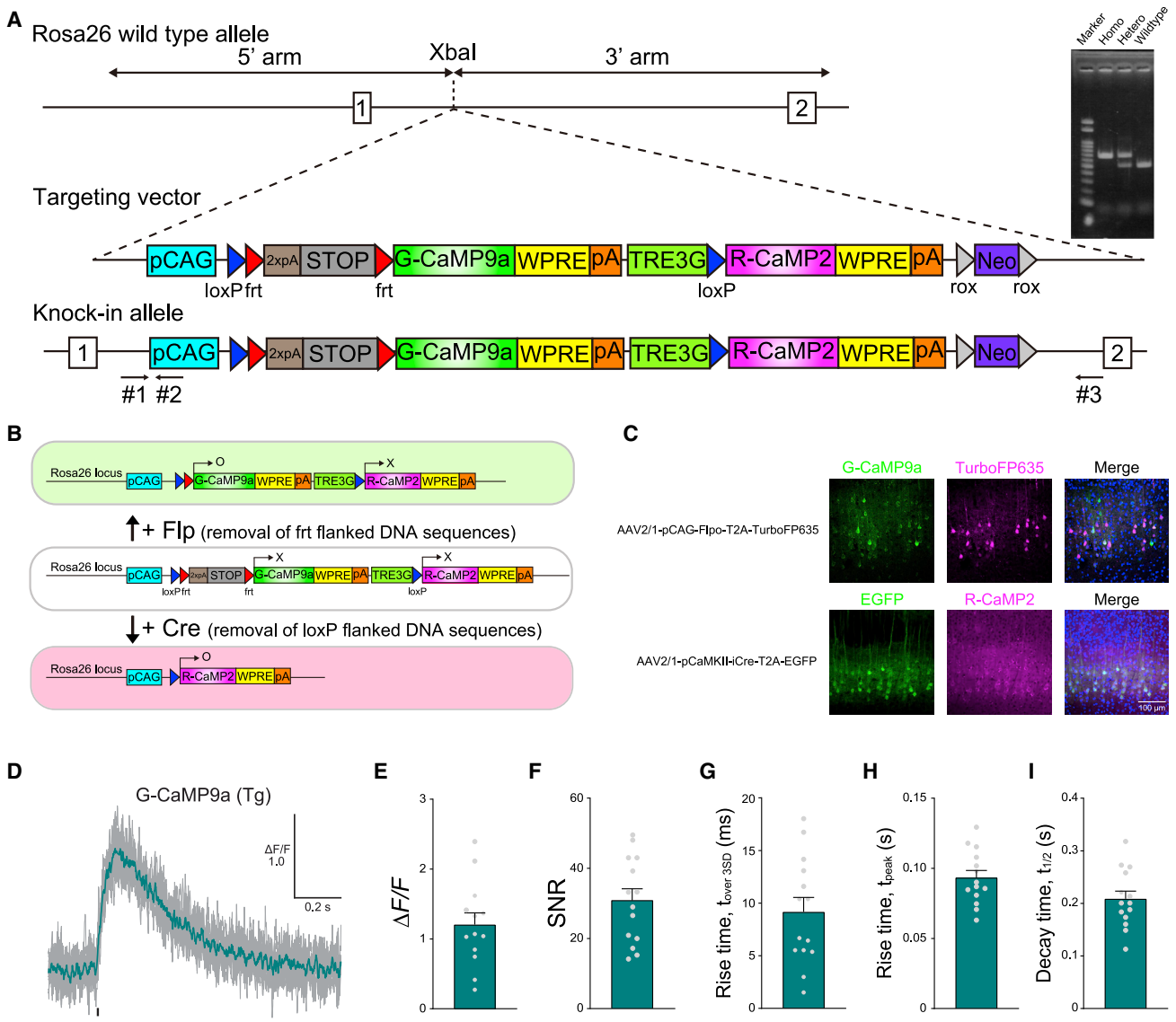

Figure 2. Generation of G-CaMP9a/R-CaMP2 knockin mouse

(A) Schematic design of the gene-targeting strategy to generate the G-CaMP9a/R-CaMP2 reporter mice. The reporter cassette (shown in between the dashed lines) was targeted to the Rosa26 locus in the intron between endogenous exons 1 and 2. Locations of the 5′ and 3′ arms for homologous recombination are indicated by the black bars. Arrows (#1–#3) show primers for PCR genotyping for G-CaMP9a/R-CaMP2 knockin mice. Primers #1 and #2 are for transgenic allele (684 bp), and primers #1 and #3 are for the wild-type allele (500 bp).

(B) Schematic diagram of interleaved control by Cre/loxP and Flp/frt recombination.

(C) Confocal images of G-CaMP9a and R-CaMP2 induced by AAV encoding Cre (AAV2/1-pCaMKII-iCre-T2A-EGFP) or Flp (AAV2/1-pCAG-Flpo-T2A-TurboFP635). Scale bar, 100 μm.

(D) Representative traces of G-CaMP9a fluorescence changes (Δ*F*/*F*) of the knockin mouse in response to a single AP of the barrel cortex layer 2/3 pyramidal neuron in an acute brain slice. The eight-trial average response of a single sweep (gray) and the averages of 8 sweeps (green) are overlaid. The black vertical line indicates stimulus.

(E–I) Mean amplitude (Δ*F*/*F*, E), SNR (F), rise time (first exceeded 3SD time point, G, and time to peak, H), and decay time constants (I) of somatic calcium transients (n = 14) by a single AP. Error bars represent SEM.

activity with cellular resolution (Figures 4F and 4G). When we examined the G-CaMP9a fluorescence of the barrel cortex in different ages, the brightness of the cytosolic G-CaMP9a was comparable between 1, 3, and 5 months of age (Figure 4H). This result suggests that transgene-derived G-CaMP9a signals are stable over months. Furthermore, there are no significant differences in the amplitudes and decay time constants of spontaneous events over time (Figures 4I and 4J). Furthermore, G-CaMP9a fluorescence was stable under continuous *in vivo* imaging for 30 min (Figure 4K). These results indicate that this

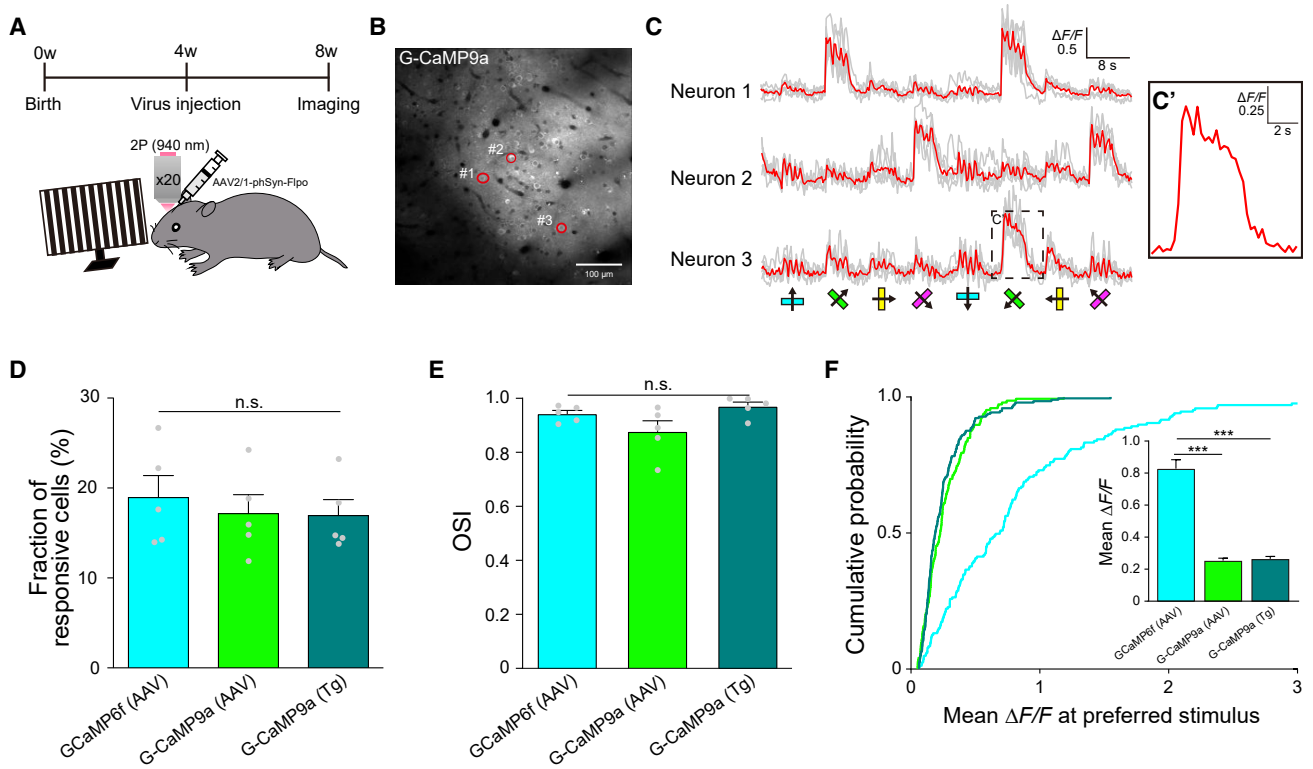

Figure 3. *In vivo* two-photon G-CaMP9a calcium imaging in layer 2/3 pyramidal neurons of the visual cortex

(A) Experimental design of *in vivo* two-photon calcium imaging of head-fixed awake mice with visual stimulation. An AAV expressing Flpo was injected at the age of 4 weeks, and *in vivo* imaging was conducted 4 weeks later.

(B) *In vivo* two-photon fluorescence image of G-CaMP9a expressing layer 2/3 pyramidal neurons in the primary visual cortex with regions of interest (#1–#3). Scale bar, 100 μm.

(C) Visual stimulus-evoked calcium transients from regions of interest (cells #1–#3 in B). Single sweeps (gray) and an average of 5 sweeps (red) are overlaid. Directions of grating motions (8 motions) are shown above traces (arrows).

(C') Higher magnification of the indicated area in (C).

(D) The fraction of cells scored as responding to visual stimulation when loaded with different calcium indicators (n = 796 cells (5 field of views (FOVs)) (GCaMP6f (AAV)), 799 cells (5 FOVs) (G-CaMP9a (AAV)), 715 cells (5 FOVs) (G-CaMP9a (Tg))). Error bars represent SEM. n.s., not significant. p = 0.8980, Kruskal-Wallis test.

(E) Average orientation selectivity index (OSI) across sensors. Error bars represent SEM. n.s., not significant. p = 0.0718, Kruskal-Wallis test.

(F) The distribution of fluorescence changes across the cells at the preferred orientation. Inset, mean Δ*F*/*F* plot. ***p < 0.001. p < 0.0001 for GCaMP6f (AAV) versus G-CaMP9a (AAV), p < 0.0001 for GCaMP6f (AAV) versus G-CaMP9a (Tg), Kolmogorov-Smirnov test. Error bars represent SEM.

knockin line can identify active neuronal ensembles in the barrel cortex and provide stable homogeneous G-CaMP9a expression without apparent adverse effects over 5 months and that they are suitable for long-term imaging.

Imaging calcium dynamics in cortical interneurons *in vivo*

Although GABAergic interneurons constitute only approximately 20% of cortical neurons, they play crucial roles in regulating the excitation/inhibition (E/I) balance, flexibility, and functional architecture of cortical circuits (Marin, 2012; Markram et al., 2004; Rubenstein and Merzenich, 2003; Tremblay et al., 2016). They have a large diversity based on morphological, molecular, and physiological properties, and these specific subclasses have been implicated in the plasticity of cortical circuits (Chen et al., 2015; Khan et al., 2018). Therefore, monitoring neuronal activity from cortical inhibitory neurons is vital to understanding machinery for generating plasticity in cortical circuits.

Thus, we next evaluated the utility of G-CaMP9a knockin mice in recording neuronal activities in cortical interneurons *in vivo*. To express G-CaMP9a in somatostatin (SOM) interneurons specifically, we used the knockin mice crossed with SOM-Flpo mice that express Flpo recombinase from SOM promoter/enhancer elements (He et al., 2016) (Figure 5A). Using these double transgenic mice, we first confirmed that almost 100% of SOM-positive neurons expressed G-CaMP9a (Figure 5B). We then conducted *in vivo* two-photon calcium imaging in layer 2/3 of the barrel cortex of SOM-Flpo; G-CaMP9a mouse in a head-fixed awake condition (Figure 5C). Consistent with prior reports, the activity of SOM-positive interneurons is highly correlated (Figures 5D–5F) (Gibson et al., 1999; Inoue et al., 2015; Karnani et al., 2016). We also found that a distinct population of SOM-positive neurons was spontaneously active but uncorrelated to other SOM-positive neurons. This result is consistent with a previous report that SOM-positive neurons may comprise distinct subpopulations (Figures 5D and 5E) (Knoblich et al., 2019). We

CellPress
OPEN ACCESS

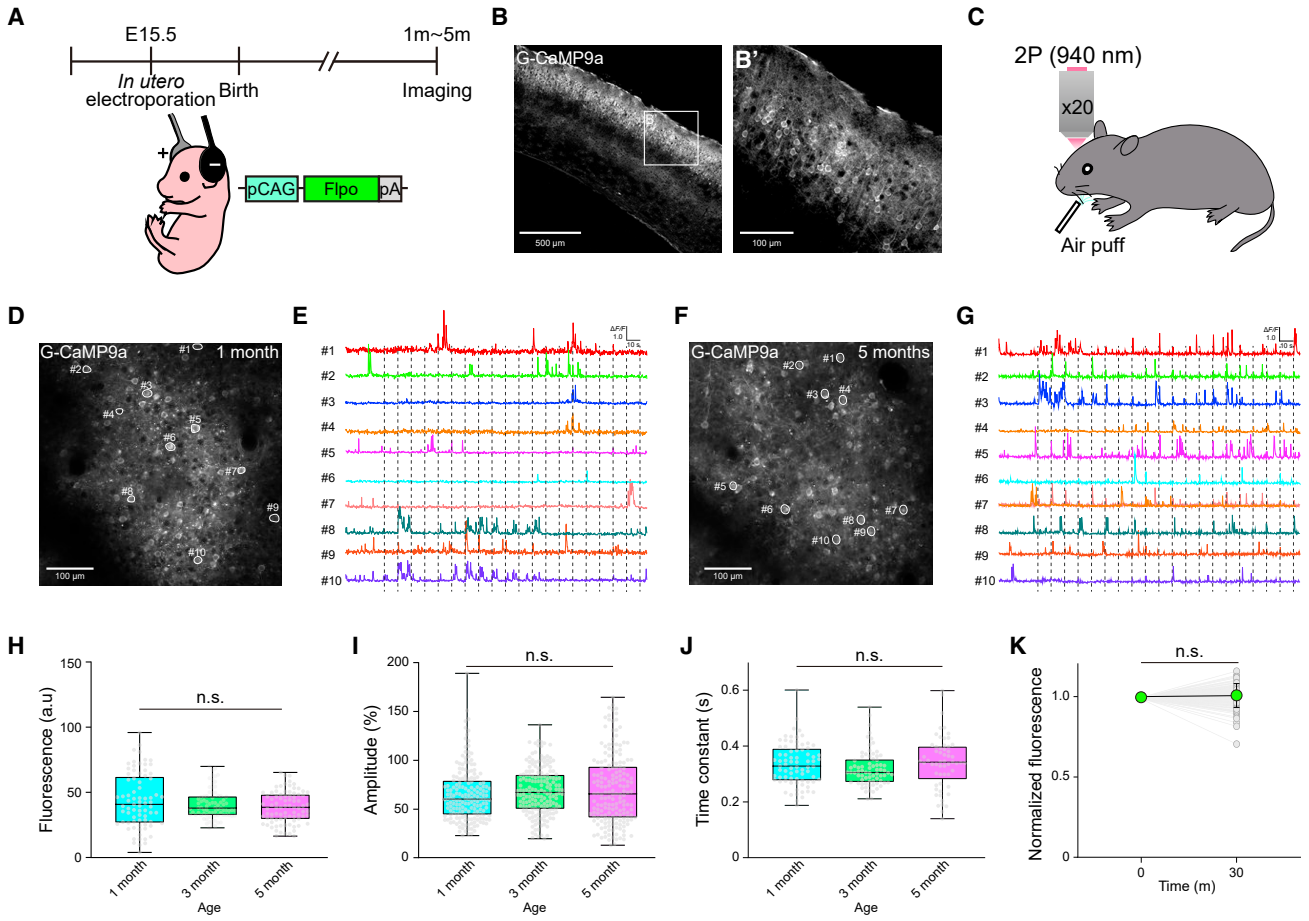

Figure 4. *In vivo* two-photon G-CaMP9a calcium imaging in layer 2/3 pyramidal neurons of the barrel cortex

(A) Experimental design of *in utero* electroporation to target layer 2/3 pyramidal neurons of the barrel cortex.

(B) Coronal section of naive G-CaMP9a fluorescence in layer 2/3 of the barrel cortex. (B′) Higher magnification of the indicated area in (B). Scale bar, 500 μm (B) and 100 μm (B′).

(C) Experimental design of *in vivo* two-photon calcium imaging of head-fixed awake mice with air-puff whisker stimulation.

(D) *In vivo* two-photon fluorescence image of G-CaMP9a expressing layer 2/3 pyramidal neurons in the barrel cortex at the age of 1 month. Scale bar, 100 μm.

(E) Whisker stimulus-evoked calcium transients from ten regions of interest (cells #1–#10 in D). Dashed lines show the timing of the whisker stimulus.

(F) *In vivo* two-photon fluorescence image of G-CaMP9a expressing layer 2/3 pyramidal neurons in the barrel cortex at the age of 5 months. Scale bar, 100 μm.

(G) Whisker stimulus-evoked calcium transients from ten regions of interest (cells #1–#10 in B). Dashed lines show the timing of the whisker stimulus.

(H–J) Quantification of neuronal brightness (H), spontaneous peak amplitude (I), and decay time constants (J). n.s., not significant. p = 0.1392 for (H), p = 0.1794 for (I), p = 0.1069 for (J), Kruskal-Wallis test.

(K) Mean fluorescence of G-CaMP9a-expressing neurons (n = 150) at 0 and 30 min during continuous two-photon *in vivo* imaging. Images were taken at 4 Hz for 30 min n.s., not significant. p = 0.1342, Wilcoxon matched signed-rank test. Error bars represent SD.

noted no strong correlation between the paired correlation coefficients across SOM-positive neurons and the distance of each soma (Figure 5G).

Dual-color calcium imaging in excitatory and inhibitory ensembles

Finally, we conducted dual-color imaging for monitoring neural activity in both excitatory and inhibitory neurons. To express G-CaMP9a specifically in GABAergic interneurons, we crossed G-CaMP9a knockin mice with Dlx5/6-Flpe transgenic mice, inducing very efficient recombination specifically in pan-GABAergic interneurons (Miyoshi et al., 2010). As described above, Cre-dependent R-CaMP2 expression from this transgenic line is too dim for *in vivo* calcium imaging. Therefore, to visualize neural activity in excitatory neurons, we injected an AAV encoding a highly sensitive and bright red GECI, XCaMP-R, in the layer 2/3 barrel cortex (Figure 6A) (Inoue et al., 2019). Using this mouse, we conducted *in vivo* calcium imaging in layer 2/3 of the barrel cortex in the head-fixed awake condition. To excite both G-CaMP9a and XCaMP-R simultaneously, a single excitation wavelength at 990 nm was used (Figure 6B). *In vivo* two-photon imaging revealed that this mouse successfully visualized the spontaneous activity of both excitatory and inhibitory neurons simultaneously (Figure 6C). Although the SNR of green GECI is maximized at 920–940 nm wavelength excitation, G-CaMP9a imaging at 990 nm showed an SNR high enough to detect

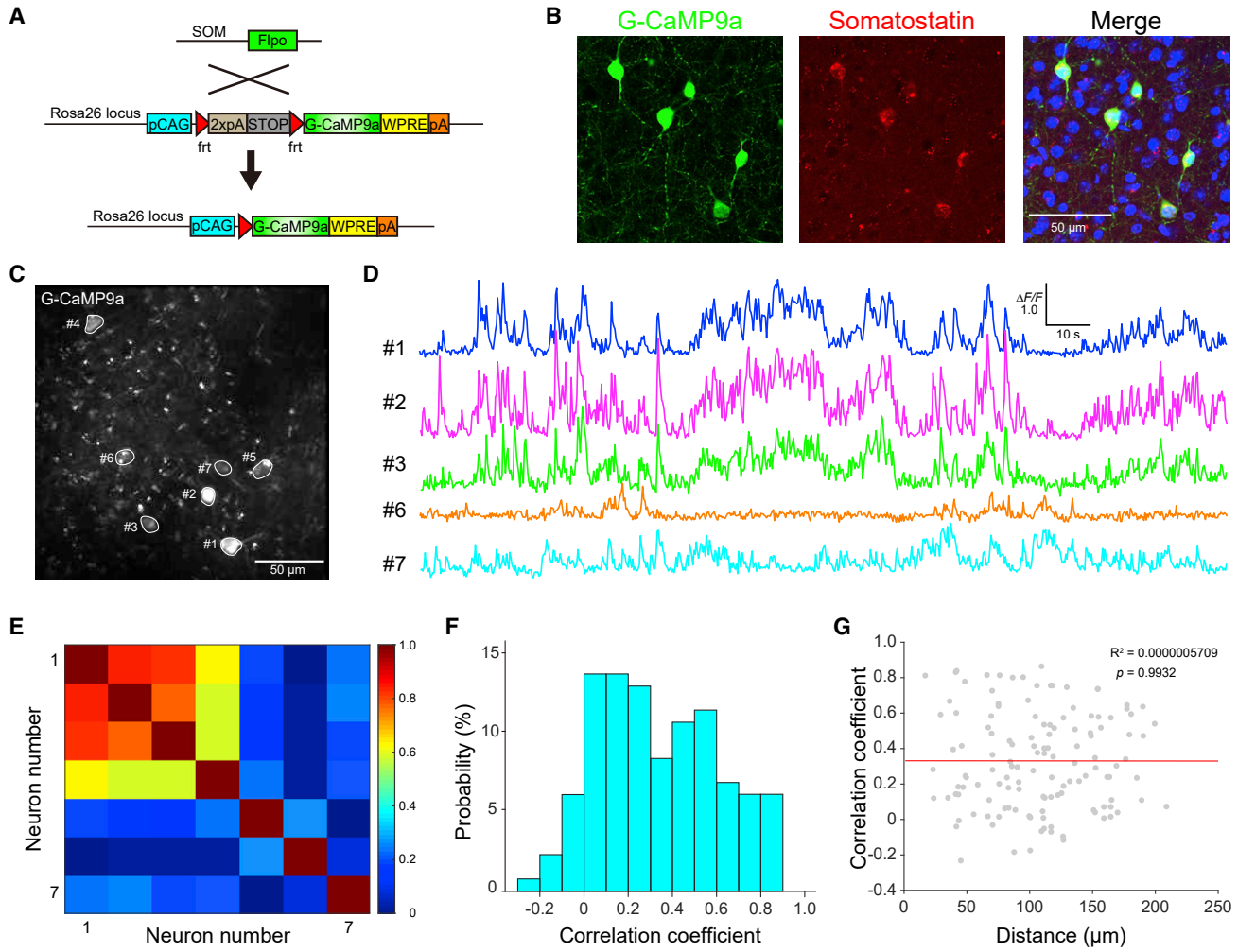

Figure 5. *In vivo* two-photon calcium imaging in layer 2/3 somatostatin positive interneurons of the barrel cortex

(A) Schematic design of genetic strategy to target somatostatin-positive interneurons.

(B) G-CaMP9a expressing coronal section of the barrel cortex immunostained with anti-somatostatin (red) antibodies.

(C) *In vivo* two-photon fluorescent image of G-CaMP9a in layer 2/3 somatostatin-positive interneurons in the barrel cortex with regions of interest (#1–#7). Scale bar, 100 μm.

(D) Spontaneous calcium transients from four regions of interest (cells #1, 2, 3, 6, and 7 in C).

(E) Correlation across all individual somatostatin-positive interneurons, as calculated from (C).

(F) Distribution of correlation coefficients across somatostatin-positive interneurons (n = 130 pairs).

(G) A plot of correlation coefficients as a function of the distance between each soma in (F). Red line shows linearly fitted line.

neuronal activity. These results suggest that the G-CaMP9a knockin mouse in combination with XCaMP-R enables investigation for complex ensemble dynamics and interactions of glutamatergic and GABAergic neurons *in vivo*.

DISCUSSION

Here, we describe the generation and validation of a knockin mouse expressing the fast and high SNR calcium indicator, G-CaMP9a, driven by a solid and ubiquitous CAG promoter targeted at the Rosa26 locus. Despite the low copy number of transgenes, our Flp-dependent G-CaMP9a transgenic line is bright and sensitive enough to detect the activity of cortical neurons *in vivo*, with a functional resolution similar to that achieved by a GECI virus injection. Also, the performance of G-CaMP9a was substantial over 5 months with high photostability. These features show that G-CaMP9a knockin mice are suitable for imaging neural activity in large neuronal populations requiring long-term observations of neural dynamics, such as during learning and other complex cognitive behaviors.

Over the past 10 years, a variety of transgenic mouse lines producing high GECI expression in selected neurons have been reported (Bethge et al., 2017; Chen et al., 2012; Daigle et al., 2018; Dana et al., 2014, 2018, 2019; Direnberger et al., 2012; Madisen et al., 2015; Sato et al., 2015; Wekselblatt et al., 2016; Zariwala et al., 2012). Most of these transgenic

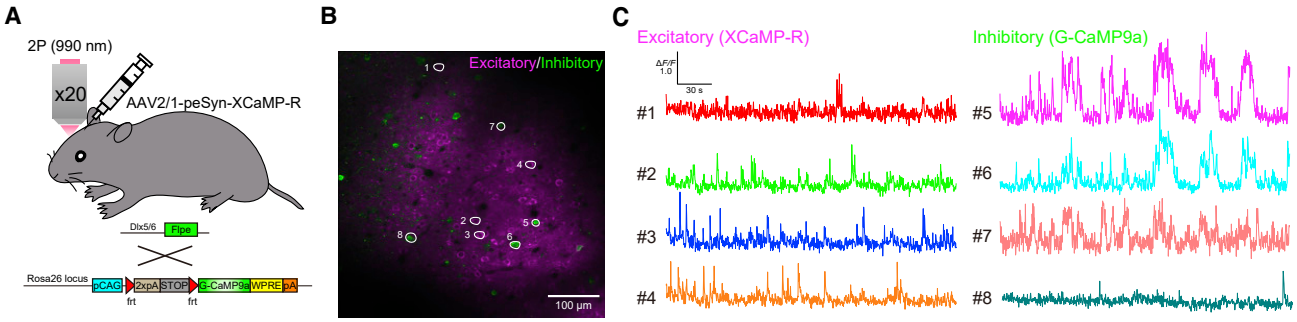

Figure 6. *In vivo* dual-color simultaneous imaging of excitatory and inhibitory neurons in the barrel cortex

(A) Experimental design of *in vivo* two-photon dual-color calcium imaging of head-fixed awake mice.

(B) *In vivo* two-photon fluorescence image of XCaMP-R-expressing excitatory neurons and G-CaMP9a-expressing inhibitory neurons in the barrel cortex with regions of interest (#1–#8). Scale bar, 100 μm.

(C) Spontaneous calcium transients from eight regions of interest (cells #1–#8 in B).

mice were designed using the Thy1 promoter or the TIGRE/tTA strategy. Thy1 promoter transgenic lines reliably achieve high-level expressions by chromosomal integration of GECI transgenes with multiple copies (Chen et al., 2012; Dana et al., 2014, 2018). However, the gene expression pattern is influenced by its location in a chromosome and its copy number. Therefore, screening multiple founder lines is indispensable. Another drawback is that the Thy1 promoter does not usually target GABAergic interneurons. Although a recent TIGRE/tTA triple-transgenic crossing strategy mostly overcame such problems, some TIGRE/tTA lines expressing a GECI showed significant abnormalities in their brain activity, including significant, broad events resembling epileptic activity, presumably due to high expression (Daigle et al., 2018; Steinmetz et al., 2017). Also, the availability of tTA driver lines is currently limited. Furthermore, tTA is a potent transcriptional transactivator that causes neurodegeneration when expressed at high levels (Han et al., 2012).

To our knowledge, this is the first example of a Flp-dependent transgenic line that can monitor neural activity faithfully from both excitatory and inhibitory neurons with cellular resolution. Our knockin mouse yields homogeneous and stable single-copy G-CaMP9a expression in selected cell populations without apparent adverse effects, having an advantage in large-area, uniform, and long-term monitoring of neuronal activities. Recently, wide-field two-photon microscopy with cellular resolution was developed to monitor neural activity in multiple cortical areas with a large field of view (Ota et al., 2021; Sofroniew et al., 2016; Stirman et al., 2016; Terada et al., 2018). This transgenic strategy can achieve wide-field GECI expression in the targeted cell population, which is difficult by viral gene delivery and *in utero* electroporation. Therefore, this knockin mouse can be useful for wide-field imaging. The development of new Flp driver lines will be a more robust strategy in refined lineage trace experiments and in the genetic manipulation of a limited number of specific neuronal populations. Consistently, the Allen Institute and other groups have started to vigorously develop new Flp-expressing transgenic lines for targeting specific cell populations (in total, about 60 kinds of Flp lines are available) (Daigle et al., 2018; He et al., 2016; Madisen et al., 2015; Miyoshi et al., 2010). By crossing it with various other Flp lines, our knockin mouse facilitates solving cell-type-specific functional networks.

Our knockin strategy can target specific populations of neurons not only in the adult brain but also in the developmental and neonatal stages, which are not accessible by virus injection and *in utero* electroporation. Also, calcium ions generate intracellular signals that control various functions in all types of cells in a biological organism, including cardiac and skeletal muscle cells. Therefore, our knockin mouse should be available for broad application in analyzing cardiac function, stem-cell development, and organogenesis.

In summary, by taking advantage of a site-specific recombination system, we have generated a G-CaMP9a knockin mouse to monitor neural activity in both excitatory and inhibitory neurons with cellular resolution. This Rosa26/CAG knockin strategy allows a homogeneous and stable expression suitable for long-term imaging in large neuronal populations. Our reporter line allows the investigation of neuronal activity in a defined population *in vivo* during learning and complex cognitive behaviors and will notably facilitate dissecting the functional dynamics and integration of neural networks.

Limitations of the study

Apart from Cre/loxP recombination, we examined R-CaMP2 expression *in vivo* under the two-photon microscopy by injecting AAV (AAV2/1-pCAG-tTA) into the visual cortex of the G-CaMP9a/R-CaMP2 knockin mouse. However, we could not see any R-CaMP2 fluorescence. It is reported that the Tet promoter in the Rosa26 locus may be affected by chromatin silencing (Godecke et al., 2017; Tasic et al., 2012). One possibility is that TetO sequence upstream of the R-CaMP2 may be heterochromatinized and not accessible for activation. Further investigation and optimization should be necessary to achieve functional calcium imaging with a red GECI driven by Rosa26/Tet transgenic strategy. Alternatively, we might resort to alternative strategies, as currently, red GECI (R-CaMP1.07 and jRGECO1a) transgenic mice can only be generated using a Cre/tTA or Thy1 promoter strategy (Bethge et al., 2017).

STAR★METHODS

Detailed methods are provided in the online version of this paper and include the following:

- KEY RESOURCES TABLE
- RESOURCE AVAILABILITY
  - Lead contact
  - Materials availability
  - Data and code availability
- EXPERIMENTAL MODEL AND SUBJECT DETAILS
  - Animals
  - Mice distribution
  - Cell lines
- METHOD DETAILS
  - Generation of G-CaMP9a
  - Protein purification
  - *In vitro* fluorometric calcium measurements
  - Measurements of extinction coefficient and quantum yield
  - Simultaneous calcium imaging and whole-cell recordings in acute brain cortical slices
  - Generation of G-CaMP9/R-CaMP2 knock-in mouse
  - *In utero* electroporation
  - AAV production and injection
  - Tissue preparation and immunohistochemistry
  - Animal surgery for *in vivo* imaging
  - *In vivo* calcium imaging
  - Sensory stimulation
  - Image analysis
- QUANTIFICATION AND STATISTICAL ANALYSIS

SUPPLEMENTAL INFORMATION

Supplemental information can be found online at https://doi.org/10.1016/j.crmeth.2022.100168.

ACKNOWLEDGMENTS

We thank the following researchers for kindly sharing their reagents: D. Kim (GCaMP6f and GCaMP6s), J. Nakai and M. Ohkura (G-CaMP4.1), G. Miyoshi and G. Fishell (Dlx5/6-Flpe mice), J. Huang (SOM-Flpo mice), and T. Takahashi and Y. Kita (fluorescence measurement at the Life Sciences Core Facility, University of Tokyo). We also thank the members of the H.B. laboratory for their support and discussion. We are particularly indebted to M. Okamura, Y. Kondo, Y. Dobashi, M. Mizukoshi, T Iwasaki, T. Kubodera, and Y. Kubota for assistance and Y. Kishida, D. Shuto, and J. Tsujimoto for animal care. This work was supported in part by grants from the Core Research for Evolutional Science and Technology Japan Science and Technology Agency (CREST-AMED) (to H.B.); Precursory Research for Embryonic Science and Technology (PRESTO)-JST (JPMJPR1906 to M.S. and JPMJPR15F6 to S.T.-K.); Grant-in-Aid for Brain Mapping by Integrated Neurotechnologies for Disease Studies (Brain/MINDS) (JP17dm0207059 to M.S., JP19dm0207080 to K.K., and JP15dm0207036 and JP19dm0207079 to H.B.); Strategic Research Program for Brain Sciences (JP16dm0107149 and JP21wm0525004 to M.S. and JP16dm0107132 to H.F.); Interstellar Initiative (JP18jm0610009 to M.S.); Brain Information Dynamics (BID) (JP17H06313 to K.K. and JP17H06312 to H.B.); JSPS KAKENHI (JP21K19429, JP20H04122, JP19H04898, JP18K19493, JP17H05941, and JP16H06728 to M.S., JP15K18372 to M.I., JP17K13270 to H.F., JP19H01007 to H.B., and JP16H06276 to M.S., M.I., and H.B.); a Comprehensive Brain Science Network (CBSN) grant from MEXT (to K.S. and H.B.); and grants from the Tokyo Society of Medical Sciences (to M.S., M.I., and H.F.), Takeda Science Foundation (to M.S., H.F., and H.B.), Uehara Memorial Foundation (to M.S.), Kowa Life Science Foundation (to M.S.), Tokyo Biochemical Research Foundation (to M.S.), Research Foundation for Opto-Science and Technology (to M.S.), Lotte Foundation (to M.S.), The Konica Minolta Science and Technology Foundation (to M.S.), Brain Science Foundation (to M.S.), Nakatani Foundation (to M.S. and H.B.), Asahi Glass Foundation (S.T.-K.), Toray Science Foundation (S.T.-K.), Astellas Foundation for Research on Metabolic Disorders (to H.F.), and Hitachi Global Foundation (to H.B). S.K. and T.Y. were supported by research fellowships from the Japan Society for the Promotion of Science for Young Scientists.

AUTHOR CONTRIBUTIONS

Conceptualization, M.S., M.I., H.F., and H.B.; methodology, M.S., M.I., S.T.-K., H.F., and H.B.; investigation, M.S., M.I., A.T., S.K., T.Y., and S.H.; resources, M.A. and K.S.; acquisition of data, M.S., M.I., A.T., and T.Y.; writing – original draft, M.S. and H.B.; writing – review & editing, M.S., M.I., and H.B.; supervision, M.K., K.K., and H.B.

DECLARATION OF INTERESTS

The authors declare no competing interests.

Received: September 2, 2021
Revised: December 9, 2021
Accepted: January 21, 2022
Published: February 14, 2022

REFERENCES

Ahrens, M.B., Orger, M.B., Robson, D.N., Li, J.M., and Keller, P.J. (2013). Whole-brain functional imaging at cellular resolution using light-sheet microscopy. Nat. Methods *10*, 413–420.

Ayzenshtat, I., Jackson, J., and Yuste, R. (2016). Orientation tuning depends on spatial frequency in mouse visual cortex. eNeuro *3*. https://doi.org/10.1523/ENEURO.0217-16.2016.

Bethge, P., Carta, S., Lorenzo, D.A., Egolf, L., Goniotaki, D., Madisen, L., Voigt, F.F., Chen, J.L., Schneider, B., Ohkura, M., et al. (2017). An R-CaMP1.07 reporter mouse for cell-type-specific expression of a sensitive red fluorescent calcium indicator. PLoS One *12*, e0179460.

Brainard, D.H. (1997). The psychophysics toolbox. Spat. Vis. *10*, 433–436.

Chen, Q., Cichon, J., Wang, W., Qiu, L., Lee, S.J., Campbell, N.R., Destefino, N., Goard, M.J., Fu, Z., Yasuda, R., et al. (2012). Imaging neural activity using Thy1-GCaMP transgenic mice. Neuron *76*, 297–308.

Chen, S.X., Kim, A.N., Peters, A.J., and Komiyama, T. (2015). Subtype-specific plasticity of inhibitory circuits in motor cortex during motor learning. Nat. Neurosci. *18*, 1109–1115.

Chen, T.W., Wardill, T.J., Sun, Y., Pulver, S.R., Renninger, S.L., Baohan, A., Schreiter, E.R., Kerr, R.A., Orger, M.B., Jayaraman, V., et al. (2013). Ultrasensitive fluorescent proteins for imaging neuronal activity. Nature *499*, 295–300.

Cossart, R., Aronov, D., and Yuste, R. (2003). Attractor dynamics of network UP states in the neocortex. Nature *423*, 283–288.

Daigle, T.L., Madisen, L., Hage, T.A., Valley, M.T., Knoblich, U., Larsen, R.S., Takeno, M.M., Huang, L., Gu, H., Larsen, R., et al. (2018). A suite of transgenic driver and reporter mouse lines with enhanced brain-cell-type targeting and functionality. Cell *174*, 465–480.e422.

Dana, H., Chen, T.W., Hu, A., Shields, B.C., Guo, C., Looger, L.L., Kim, D.S., and Svoboda, K. (2014). Thy1-GCaMP6 transgenic mice for neuronal population imaging in vivo. PLoS One *9*, e108697.

Dana, H., Mohar, B., Sun, Y., Narayan, S., Gordus, A., Hasseman, J.P., Tsegaye, G., Holt, G.T., Hu, A., Walpita, D., et al. (2016). Sensitive red protein calcium indicators for imaging neural activity. Elife *5*, e12727.

Dana, H., Novak, O., Guardado-Montesino, M., Fransen, J.W., Hu, A., Borghuis, B.G., Guo, C., Kim, D.S., and Svoboda, K. (2018). Thy1 transgenic

mice expressing the red fluorescent calcium indicator jRGECO1a for neuronal population imaging in vivo. PLoS One *13*, e0205444.

Dana, H., Sun, Y., Mohar, B., Hulse, B.K., Kerlin, A.M., Hasseman, J.P., Tsegaye, G., Tsang, A., Wong, A., Patel, R., et al. (2019). High-performance calcium sensors for imaging activity in neuronal populations and microcompartments. Nat. Methods *16*, 649–657.

Direnberger, S., Mues, M., Micale, V., Wotjak, C.T., Dietzel, S., Schubert, M., Scharr, A., Hassan, S., Wahl-Schott, C., Biel, M., et al. (2012). Biocompatibility of a genetically encoded calcium indicator in a transgenic mouse model. Nat. Commun. *3*, 1031.

Dombeck, D.A., Harvey, C.D., Tian, L., Looger, L.L., and Tank, D.W. (2010). Functional imaging of hippocampal place cells at cellular resolution during virtual navigation. Nat. Neurosci. *13*, 1433–1440.

Gibson, J.R., Beierlein, M., and Connors, B.W. (1999). Two networks of electrically coupled inhibitory neurons in neocortex. Nature *402*, 75–79.

Godecke, N., Zha, L., Spencer, S., Behme, S., Riemer, P., Rehli, M., Hauser, H., and Wirth, D. (2017). Controlled re-activation of epigenetically silenced Tet promoter-driven transgene expression by targeted demethylation. Nucleic Acids Res. *45*, e147.

Han, H.J., Allen, C.C., Buchovecky, C.M., Yetman, M.J., Born, H.A., Marin, M.A., Rodgers, S.P., Song, B.J., Lu, H.C., Justice, M.J., et al. (2012). Strain background influences neurotoxicity and behavioral abnormalities in mice expressing the tetracycline transactivator. J. Neurosci. *32*, 10574–10586.

He, M., Tucciarone, J., Lee, S., Nigro, M.J., Kim, Y., Levine, J.M., Kelly, S.M., Krugikov, I., Wu, P., Chen, Y., et al. (2016). Strategies and tools for combinatorial targeting of GABAergic neurons in mouse cerebral cortex. Neuron *91*, 1228–1243.

Huber, D., Gutnisky, D.A., Peron, S., O'Connor, D.H., Wiegert, J.S., Tian, L., Oertner, T.G., Looger, L.L., and Svoboda, K. (2012). Multiple dynamic representations in the motor cortex during sensorimotor learning. Nature *484*, 473–478. https://doi.org/10.1038/nature11039.

Imayoshi, I., Hirano, K., Sakamoto, M., Miyoshi, G., Imura, T., Kitano, S., Miyachi, H., and Kageyama, R. (2012). A multifunctional teal-fluorescent Rosa26 reporter mouse line for Cre- and Flp-mediated recombination. Neurosci. Res. *73*, 85–91.

Inoue, M., Takeuchi, A., Horigane, S., Ohkura, M., Gengyo-Ando, K., Fujii, H., Kamijo, S., Takemoto-Kimura, S., Kano, M., Nakai, J., et al. (2015). Rational design of a high-affinity, fast, red calcium indicator R-CaMP2. Nat. Methods *12*, 64–70.

Inoue, M., Takeuchi, A., Manita, S., Horigane, S.I., Sakamoto, M., Kawakami, R., Yamaguchi, K., Otomo, K., Yokoyama, H., Kim, R., et al. (2019). Rational engineering of XCaMPs, a multicolor GECI suite for in vivo imaging of complex brain circuit dynamics. Cell *177*, 1346–1360.

Karnani, M.M., Jackson, J., Ayzenshtat, I., Tucciarone, J., Manoocheri, K., Snider, W.G., and Yuste, R. (2016). Cooperative subnetworks of molecularly similar interneurons in mouse neocortex. Neuron *90*, 86–100.

Kato, H.K., Chu, M.W., Isaacson, J.S., and Komiyama, T. (2012). Dynamic sensory representations in the olfactory bulb: modulation by wakefulness and experience. Neuron *76*, 962–975.

Khan, A.G., Poort, J., Chadwick, A., Blot, A., Sahani, M., Mrsic-Flogel, T.D., and Hofer, S.B. (2018). Distinct learning-induced changes in stimulus selectivity and interactions of GABAergic interneuron classes in visual cortex. Nat. Neurosci. *21*, 851–859.

Knoblich, U., Huang, L., Zeng, H., and Li, L. (2019). Neuronal cell-subtype specificity of neural synchronization in mouse primary visual cortex. Nat. Commun. *10*, 2533.

Komiyama, T., Sato, T.R., O'Connor, D.H., Zhang, Y.X., Huber, D., Hooks, B.M., Gabitto, M., and Svoboda, K. (2010). Learning-related fine-scale specificity imaged in motor cortex circuits of behaving mice. Nature *464*, 1182–1186.

Madisen, L., Garner, A.R., Shimaoka, D., Chuong, A.S., Klapoetke, N.C., Li, L., van der Bourg, A., Niino, Y., Egolf, L., Monetti, C., et al. (2015). Transgenic mice for intersectional targeting of neural sensors and effectors with high specificity and performance. Neuron *85*, 942–958.

Madisen, L., Zwingman, T.A., Sunkin, S.M., Oh, S.W., Zariwala, H.A., Gu, H., Ng, L.L., Palmiter, R.D., Hawrylycz, M.J., Jones, A.R., et al. (2010). A robust and high-throughput Cre reporting and characterization system for the whole mouse brain. Nat. Neurosci. *13*, 133–140.

Marin, O. (2012). Interneuron dysfunction in psychiatric disorders. Nat. Rev. Neurosci. *13*, 107–120.

Markram, H., Toledo-Rodriguez, M., Wang, Y., Gupta, A., Silberberg, G., and Wu, C. (2004). Interneurons of the neocortical inhibitory system. Nat. Rev. Neurosci. *5*, 793–807.

Mishina, M., and Sakimura, K. (2007). Conditional gene targeting on the pure C57BL/6 genetic background. Neurosci. Res. *58*, 105–112.

Miyoshi, G., Hjerling-Leffler, J., Karayannis, T., Sousa, V.H., Butt, S.J., Battiste, J., Johnson, J.E., Machold, R.P., and Fishell, G. (2010). Genetic fate mapping reveals that the caudal ganglionic eminence produces a large and diverse population of superficial cortical interneurons. J. Neurosci. *30*, 1582–1594.

Mrsic-Flogel, T.D., Hofer, S.B., Ohki, K., Reid, R.C., Bonhoeffer, T., and Hubener, M. (2007). Homeostatic regulation of eye-specific responses in visual cortex during ocular dominance plasticity. Neuron *54*, 961–972.

Nakai, J., Ohkura, M., and Imoto, K. (2001). A high signal-to-noise Ca^{2+} probe composed of a single green fluorescent protein. Nat. Biotechnol. *19*, 137–141.

Niell, C.M., and Stryker, M.P. (2008). Highly selective receptive fields in mouse visual cortex. J. Neurosci. *28*, 7520–7536.

O'Connor, D.H., Peron, S.P., Huber, D., and Svoboda, K. (2010). Neural activity in barrel cortex underlying vibrissa-based object localization in mice. Neuron *67*, 1048–1061.

Ohki, K., Chung, S., Ch'ng, Y.H., Kara, P., and Reid, R.C. (2005). Functional imaging with cellular resolution reveals precise micro-architecture in visual cortex. Nature *433*, 597–603.

Ohkura, M., Sasaki, T., Sadakari, J., Gengyo-Ando, K., Kagawa-Nagamura, Y., Kobayashi, C., Ikegaya, Y., and Nakai, J. (2012). Genetically encoded green fluorescent Ca^{2+} indicators with improved detectability for neuronal Ca^{2+} signals. PLoS One *7*, e51286.

Ota, K., Oisi, Y., Suzuki, T., Ikeda, M., Ito, Y., Ito, T., Uwamori, H., Kobayashi, K., Kobayashi, M., Odagawa, M., et al. (2021). Fast, cell-resolution, contiguous-wide two-photon imaging to reveal functional network architectures across multi-modal cortical areas. Neuron *109*, 1810–1824 e1819.

Pachitariu, M., Stringer, C., Dipoppa, M., Schröder, S., Rossi, L.F., Dalgleish, H., Carandini, M., and Harris, K.D. (2017). Suite2p: beyond 10,000 neurons with standard two-photon microscopy. bioRxiv. https://doi.org/10.1101/061507v2.

Peters, A.J., Chen, S.X., and Komiyama, T. (2014). Emergence of reproducible spatiotemporal activity during motor learning. Nature *510*, 263–267.

Rubenstein, J.L., and Merzenich, M.M. (2003). Model of autism: increased ratio of excitation/inhibition in key neural systems. Genes Brain Behav. *2*, 255–267.

Sakamoto, M., Ieki, N., Miyoshi, G., Mochimaru, D., Miyachi, H., Imura, T., Yamaguchi, M., Fishell, G., Mori, K., Kageyama, R., and Imayoshi, I. (2014). Continuous postnatal neurogenesis contributes to formation of the olfactory bulb neural circuits and flexible olfactory associative learning. J. Neurosci. *34*, 5788–5799.

Sato, M., Kawano, M., Ohkura, M., Gengyo-Ando, K., Nakai, J., and Hayashi, Y. (2015). Generation and imaging of transgenic mice that express G-CaMP7 under a tetracycline response element. PLoS One *10*, e0125354.

Shindo, A., Hara, Y., Yamamoto, T.S., Ohkura, M., Nakai, J., and Ueno, N. (2010). Tissue-tissue interaction-triggered calcium elevation is required for cell polarization during Xenopus gastrulation. PLoS One *5*, e8897.

Sofroniew, N.J., Flickinger, D., King, J., and Svoboda, K. (2016). A large field of view two-photon mesoscope with subcellular resolution for in vivo imaging. Elife *5*, e14472.

Soriano, P. (1999). Generalized lacZ expression with the ROSA26 Cre reporter strain. Nat. Genet. *21*, 70–71.

Steinmetz, N.A., Buetfering, C., Lecoq, J., Lee, C.R., Peters, A.J., Jacobs, E.A.K., Coen, P., Ollerenshaw, D.R., Valley, M.T., de Vries, S.E.J., et al. (2017). Aberrant cortical activity in multiple GCaMP6-expressing transgenic mouse lines. eNeuro *4*. https://doi.org/10.1523/ENEURO.0207-17.2017.

Stirman, J.N., Smith, I.T., Kudenov, M.W., and Smith, S.L. (2016). Wide field-of-view, multi-region, two-photon imaging of neuronal activity in the mammalian brain. Nat. Biotechnol. *34*, 857–862.

Tada, M., Takeuchi, A., Hashizume, M., Kitamura, K., and Kano, M. (2014). A highly sensitive fluorescent indicator dye for calcium imaging of neural activity in vitro and in vivo. Eur. J. Neurosci. *39*, 1720–1728.

Tasic, B., Miyamichi, K., Hippenmeyer, S., Dani, V.S., Zeng, H., Joo, W., Zong, H., Chen-Tsai, Y., and Luo, L. (2012). Extensions of MADM (mosaic analysis with double markers) in mice. PLoS One *7*, e33332.

Terada, S.I., Kobayashi, K., Ohkura, M., Nakai, J., and Matsuzaki, M. (2018). Super-wide-field two-photon imaging with a micro-optical device moving in post-objective space. Nat. Commun. *9*, 3550.

Thevenaz, P., Ruttimann, U.E., and Unser, M. (1998). A pyramid approach to subpixel registration based on intensity. IEEE Trans. Image Process. *7*, 27–41.

Tian, L., Hires, S.A., Mao, T., Huber, D., Chiappe, M.E., Chalasani, S.H., Petreanu, L., Akerboom, J., McKinney, S.A., Schreiter, E.R., et al. (2009). Imaging neural activity in worms, flies and mice with improved GCaMP calcium indicators. Nat. Methods *6*, 875–881.

Tremblay, R., Lee, S., and Rudy, B. (2016). GABAergic interneurons in the neocortex: from cellular properties to circuits. Neuron *91*, 260–292. https://doi.org/10.1016/j.neuron.2016.06.033.

Wekselblatt, J.B., Flister, E.D., Piscopo, D.M., and Niell, C.M. (2016). Large-scale imaging of cortical dynamics during sensory perception and behavior. J. Neurophysiol. *115*, 2852–2866.

Zariwala, H.A., Borghuis, B.G., Hoogland, T.M., Madisen, L., Tian, L., De Zeeuw, C.I., Zeng, H., Looger, L.L., Svoboda, K., and Chen, T.W. (2012). A Cre-dependent GCaMP3 reporter mouse for neuronal imaging in vivo. J. Neurosci. *32*, 3131–3141.

Zhao, Y., Araki, S., Wu, J., Teramoto, T., Chang, Y.F., Nakano, M., Abdelfattah, A.S., Fujiwara, M., Ishihara, T., Nagai, T., and Campbell, R.E. (2011). An expanded palette of genetically encoded Ca^{2+} indicators. Science *333*, 1888–1891.

STAR★METHODS

KEY RESOURCES TABLE

REAGENT or RESOURCE	SOURCE	IDENTIFIER
Antibodies		
Rabbit polyclonal anti-GFP	Thermo Fisher Scientific	Cat# A11122; RRID: AB_221569
Rat monoclonal anti-GFP	Nacalai tesque	Cat# 04404-84; RRID: AB_10013361
Rat monoclonal anti-RFP	Chromotek	Cat# 5f8-100; RRID: AB_ 2336064
Rabbit polyclonal anti- TurboFP635	Evrogen	Cat# AB233; RRID: AB_ 2571743
Rat polyclonal anti-somatostatin	Millipore	Cat# MAB354; RRID: AB 2255365
Bacterial and virus strains		
AAV2/1-pCaMKIIα-iCre-T2A-EGFP	This paper	N/A
AAV2/1-pCAG-Flpo-T2A-TurboFP635	This paper	N/A
AAV2/1-pCAG-tTA	This paper	N/A
AAV2/1-phSyn-Flpo	This paper	N/A
AAV2/1-pCaMKIIα-GCaMP6f	This paper	N/A
AAV2/1-pCaMKIIα-G-CaMP9a	This paper	RIKEN BRC: RDB19172
AAV2/1-peSyn-XCaMP-R	This paper	N/A
Chemicals, peptides, and recombinant proteins		
Hoechst 33342	Thermo Fisher Scientific	Cat# H3570
G-CaMP9a	This paper	Genbank: LC654935
Critical commercial assays		
Calcium Calibration Buffer Kit#1	Thermo Fisher Scientific	Cat# C3008MP
SYBR qPCR: SYBR Premix Ex Taq (Tli RNase H Plus)	Clontech	Cat# RR420
NucleoBond Xtra Midi EF	MACHEREY-NAGEL	Cat# 740420
Experimental models: Cell lines		
HEK293T	ATCC	Cat# CRL-11268
Sf9	Thermo Fisher Scientific	Cat# B82501
KRX	Promega	Cat# L3002
DH5α	TOYOBO	Cat# DNA-903
RENKA ES	Mishina and Sakimura (2007)	N/A
Experimental models: Organisms/strains		
Mouse: ICR	Japan SLC	N/A
Mouse: C57BL/6N	Japan SLC	N/A
Mouse: SOM-Flpo (Sst$^{tm3.1(flpo)Zjh}$/J)	Jackson Laboratory	Cat#028579
Mouse: Dlx5/6-Flpe (Tg(mI56i-flpe)39Fsh/J)	Jackson Laboratory	Cat#010815
Mouse: G-CaMP9a (C57BL/6N-Gt(ROSA)26Sor<tm1 (CAG-G-CaMP9a,-R-CaMP2)Hbto>)	This paper	RIKEN BRC: RBRC11575
Oligonucleotides		
Rosa26 forward primer 5′-AGTCGCTCTGAGTTGTTATC-3′	This paper	N/A
Rosa26 reverse primer 5′-GGATCTCAAGCAGGAGAGTA-3′	This paper	N/A
pCAG reverse primer 5′-GATGGGGAGAGTGAAGCAGAACGT-3′	This paper	N/A
Recombinant DNA		
pTRE$_{tight}$-GCaMP6f	Inoue et al. (2019)	N/A
pTRE$_{tight}$-GCaMP6s	Inoue et al. (2019)	N/A
pTRE$_{tight}$-G-CaMP9a	This paper	N/A
pCAG-TetOn3G	Inoue et al. (2015)	N/A

(*Continued on next page*)

Continued

REAGENT or RESOURCE	SOURCE	IDENTIFIER
pRSET-GCaMP6f	Inoue et al. (2019)	N/A
pRSET-GCaMP6s	Inoue et al. (2019)	N/A
pRSET-G-CaMP9a	This paper	N/A
pCAG-Flpo	This paper	N/A
Software and algorithms		
MATLAB	Mathworks	http://Mathworks.com
GraphPad Prism 9	GraphPad	http://Graphpad.com
ImageJ	NIH	https://imagej.nih.gov/ij/
Origin Pro 7.5	Origin Lab	http://Originlab.com

RESOURCE AVAILABILITY

Lead contact

Further information and requests for resources and reagents should be directed to and will be fulfilled by the lead contact, Haruhiko Bito (hbito@m.u-tokyo.ac.jp).

Materials availability

A plasmid generated in this study have been deposited to the RIKEN BRC (catalog number: RDB19172). A mouse line generated in this study have been deposited to the RIKEN BRC (catalog number: RBRC11575).

Data and code availability

- All data reported in this paper will be shared by the lead contact upon request.
- This paper does not report original code.
- Any additional information required to reanalyze the data reported in this paper is available from the lead contact upon request.

EXPERIMENTAL MODEL AND SUBJECT DETAILS

Animals

All animals were handled in accordance with the University of Tokyo Guide and the Niigata University Guide for the Care and Use of Laboratory Animals. Wild-type, SOM-Flpo (Jackson Laboratory stock No. 028579) (He et al., 2016), Dlx5/6-Flpe (Jackson Laboratory stock No. 010815) (Miyoshi et al., 2010), and G-CaMP9a/R-CaMP2 transgenic lines were group-housed and kept on a 12-h light/dark cycle with *ad libitum* food and water at room temperature. Wild-type animals used in this study were purchased from Japan SLC. Experiments were performed with reporter mice of either sex between 3 and 20 weeks of age.

Mice distribution

The G-CaMP9a/R-CaMP2 knock-in line was deposited to the RIKEN BRC (http://mus.brc.riken.jp/en/) for distribution. The repository stock number is RBRC11575. Frozen embryos of the knock-in strain are available.

Cell lines

HEK293T cells were obtained from the American Type Culture Collection (CRL-11268). Cells were cultured in Dulbecco's Modified Eagle's Medium (DMEM) (Sigma-Aldrich) supplemented with 10% fetal bovine serum (FBS) (Japan Bioserum), 50 units/ml penicillin and 50 μg/ml streptomycin (Thermo Fisher Scientific) at 37°C, 5% CO_2 in a humidified atmosphere. Sf9 cells were obtained from Thermo Fisher Scientific (B82501). Cells were cultured under suspension condition in Grace's Insect Medium (Thermo Fisher Scientific) supplemented with 10% FBS (Japan Bioserum), Sf-900 II SFM (Thermo Fisher Scientific) with 5% FBS (Japan Bioserum), 37.5 units/ml penicillin and 37.5 μg/ml streptomycin (Thermo Fisher Scientific) at 28°C. E. Coli DH5α and KRX cells were obtained from TOYOBO (DNA-903) and Promega (L3002), respectively. Bacteria were incubated in Lysogeny Broth medium supplemented with antibiotics at 37°C. RENKA embryonic stem (ES) cells were isolated from C57BL/6N mouse blastocyst (Mishina and Sakimura, 2007). Cells were cultured in KnockOut DMEM (Thermo Fisher Scientific) supplemented with 17.7% KnockOut Serum Replacement (Thermo Fisher Scientific), 3.18 mM L-glutamine, 88.4 μM non-essential amino acids, 88.4 μM 2-mercaptoethanol (Sigma-Aldrich), and 884 U/ml murine leukemia inhibitory factor (LIF) (Sigma-Aldrich) at 37°C, 5% CO2 in a humidified atmosphere.

CellPress
OPEN ACCESS

METHOD DETAILS

Generation of G-CaMP9a

G-CaMP4.1 expression construct was obtained from Dr. Junichi Nakai. We deleted the N-terminal arginine immediately after the initiator methionine of G-CaMP4.1 to enhance baseline fluorescence (Tian et al., 2009). To generate G-CaMP9a, the M13 sequence of G-CaMP4.1 was replaced with a Ca^{2+}/CaM-binding peptide derived from rat CaMKKa Val438-Phe463 (ckkap). The GENBANK accession number for the sequence of G-CaMP9a is LC654935. G-CaMP9a plasmid was deposited to the RIKEN BRC (https://dna.brc.riken.jp/en/) for distribution. The repository stock number is RDB19172.

Protein purification

Expression of recombinant proteins in *E. coli*, and their purification were performed as previously described (Inoue et al., 2015). Briefly, *E. coli* KRX (Promega) transformed with bacterial expression plasmids for G-CaMP9a was grown at 37°C. Protein expression was induced by the addition of 0.1% rhamnose and by incubating for an additional 40 h at 20°C. The GECI proteins were purified with N-terminal histidine tags, dialyzed into a storage buffer (20 mM MOPS (pH 7.2), 100 mM KCl, 1 mM DTT) and subjected to *in vitro* characterization of quantum yield and pH titration.

In vitro fluorometric calcium measurements

In vitro fluorometry was performed in 96-well plates (PerkinElmer) using a Fusion α plate reader (PerkinElmer) at room temperature. Filter sets used for fluorescent measurement for green calcium indicators were ET495/10x (Chroma) (excitation) and FF02-520/28 (Semrock) (emission). The dynamic range was calculated as $\Delta F/F$. $\Delta F/F$ was calculated as $(F_{max}–F_0)/F_0$, where F_{max} is the fluorescence intensity at a saturating $[Ca^{2+}]$ of 0.3 mM and F_0 is the fluorescence intensity measured at zero $[Ca^{2+}]$ in the presence of 15 mM EGTA. Calcium titration experiments were performed by mixing 10 mM solutions of K_2H_2EGTA and Ca_2EGTA proportionally from Calcium Calibration Buffer Kit #1 (Thermo Fisher Scientific). The K_d value and Hill coefficient were calculated by fitting according to the Hill equation using Origin Pro 7.5 (Origin Lab).

Measurements of extinction coefficient and quantum yield

Quantum yields (%sat) of Ca^{2+}-saturated G-CaMP9a in 20mM MOPS, 100mM KCl, 1mM $CaCl_2$ were measured directly with an integrating-sphere spectrometer (Quantaurus-QY, Hamamatsu). Absorbance and fluorescence emission spectra were measured in the KM buffer (100 mM KCl and 20 mM MOPS, pH 7.2) with 15 mM EGTA or 1 mM Ca^{2+}-EGTA (SpectraMax M2, Molecular Devices).

Extinction coefficients (ε) were determined by measuring the absorption spectrum of each GECI in the KM buffer (100 mM KCl and 20 mM MOPS, pH 7.2) with 1 mM EGTA or 1 mM Ca^{2+}-EGTA. The concentration of each GECI was determined by measuring SDS-PAGE stained with CBB comparison to BSA as a standard.

Simultaneous calcium imaging and whole-cell recordings in acute brain cortical slices

Acute brain slice experiments were performed as previously described (Inoue et al., 2019). Mice of either sex were sacrificed by rapid decapitation after anesthesia with CO_2. The brains were immediately extracted and immersed in gassed (95% O_2/5% CO_2) and ice-cold artificial cerebrospinal fluid (ACSF) containing (in mM); 125 NaCl, 2.5 KCl, 1.25 NaH_2PO_4, 26 $NaHCO_3$, 2 $CaCl_2$, 1 $MgCl_2$, 25 glucose. Acute coronal brain slices (200–250 μm thick) of the barrel cortex were cut in gassed, ice-cold ACSF with a vibratome (VT1200S; Leica). Brain slices were then transferred to an incubation chamber containing gassed ACSF at 30°C for 30 min and subsequently maintained at room temperature before transferring them to the recording chamber.

Whole-cell recordings were performed in the layer 2/3 pyramidal neurons of the barrel cortex with glass recording electrodes (5–8 MΩ) filled with the intracellular solution containing (in mM): 133 K-$MeSO_3$, 7.4 KCl, 10 HEPES, 3 Na_2ATP, 0.3 Na_2GTP, 0.3 $MgCl_2$. Amplifier control and data acquisition of current-clamp recordings were performed using an EPC10 amplifier (Heka Elektronik) filtered at 10 kHz and sampled at 20 kHz. During recordings, the temperature in the chamber was maintained at 30°C with oxygenated ACSF.

Calcium imaging was conducted with a two-photon microscope (FV1000-MPE, Olympus) using a 25x/1.05 N.A. water immersion objective and tunable Ti: Sapphire laser (MaiTai HP DeepSee, Spectra-Physics). Photomultiplier tubes (Hamamatsu) were used to detect the emitted light. The laser was tuned to 940 nm. The laser powers used were 23–35 mW at the front aperture of the objective. Line scanning was conducted on the soma of the pyramidal neurons (sampling rate = 774 Hz). APs were evoked by injecting a series of current pulses (0.8 nA, 2 ms duration, 1–8 pulses at 1–40 Hz) through the patch pipette. Each trial was repeated eight times, and the mean value was presented

Generation of G-CaMP9/R-CaMP2 knock-in mouse

The targeting vector contains a splice CAG promoter, frt-franked repeated SV40 polyadenylation signal (pA), STOP cassette containing the terminator of the yeast His3 gene, SV40 pA signal, G-CaMP9a-WPRE-bGHpA, R-CaMP2-WPRE-hGHpA, and rox-flanked pPGK-Neo cassette. The TRE3G sequence (Clontech) is inserted after the G-CaMP9a-WPRE-bGHpA. Two loxP sites are inserted before the repeated SV40pA signal and after the TRE3G sequence. This vector also has 5′ and 3′ homology arms of 4.7- and 5.2-kbp, respectively, which target the construct to the Xba1 site of intron 1 at the Rosa26 locus.

The targeting vector was linearized and electroporated into the RENKA C57BL/6 embryonic stem cell line (Mishina and Sakimura, 2007). G418-resistant ES clones were screened by southern blot analysis for homologous recombination at the Rosa26 by probing SpeI-digested genomic DNA with a 0.4 kb genomic fragment from immediately upstream of the 5′ arm and EcoRI-digested genomic DNA with a 0.6 kb genomic fragment from immediately downstream of the 3′ arm.

Targeted ES clones were injected into eight-cell stage ICR, which were cultured to produce blastocysts and later transferred to pseudopregnant ICR females. The resulting male chimeric mice were crossed with female C57BL/6 mice to establish the G-CaMP9a/R-CaMP2 line. The G-CaMP9a/R-CaMP2 knock-in mice used in this study still contain the PGK-Neo cassette downstream of the expression cassette because previous studies showed no expression differences between Rosa26 reporter lines with and without the PGK-Neo cassette (Madisen et al., 2010; Zariwala et al., 2012).

Genotyping of the knock-in mice was determined by PCR using the following oligonucleotides: Rosa26 forward primer (5′-AGTCGCTCTGAGTTGTTATC-3′), Rosa26 reverse primer (5′-GGATCTCAAGCAGGAGAGTA-3′), pCAG reverse primer (5′-GATGGGGAGAGTGAAGCAGAACGT-3′). Rosa26 forward primer and Rosa26 reverse primer correspond to the wild-type Rosa26 locus, and pCAG reverse primer corresponds to the transgene. Rosa26 forward primer and Rosa26 reverse primer amplified a 500-bp fragment specific to the wild-type allele. Rosa26 forward primer and pCAG reverse primer amplified a 684-bp fragment specific to the knock-in allele.

In utero electroporation

Pregnant mice were anesthetized with sodium pentobarbital (90 mg/kg; Kyoritsu), and uterine horns were exposed by laparotomy. The plasmid mixed with Fast Green (0.05% w/v; Sigma-Aldrich) for visually tracking injection location was injected through the uterine wall into the left lateral ventricle of each embryo through the uterine wall using a pulled glass capillary. For validating GECIs (Figure 1), the tetracycline-inducible expression system using a TRE_{tight} promoter and Tet-On3G constructs (Clontech) (2.5–3.0 μg/μl in final concentration) were used for green GECIs expression at embryonic day 14.5 (E14.5) ICR mice. For validating G-CaMP9a (Figure 2) and *in vivo* calcium imaging (Figures 4 and S2), pCAG-Flpo plasmid (1.0 μg/μl in final concentration) was used for G-CaMP9a expression at E12.5 or 15.5 G-CaMP9a/R-CaMP2 knock-in mice. After soaking the uterine horn with warm saline (37°C), each embryo's head was carefully held between tweezers with platinum 5 mm disk electrodes (CUY650P5, Nepa Gene). Subsequently, five electrical pulses (45 V, 50 ms duration at 1 Hz) were delivered by an electroporator (ECM 830, BTX). After the electroporation, the uterine horns were returned into the abdominal cavity, and the skin was closed with sutures. Electroporated mice were used for simultaneous calcium imaging and whole-cell recordings in acute brain slices 3–7 weeks after birth and *in vivo* calcium imaging 1–5 months after birth. In the tetracycline-inducible expression system, mice were given water containing doxycycline (10 mg/ml) in 2% sucrose in drinking water 5–7 days before the experiment.

AAV production and injection

All recombinant AAV were produced using the baculovirus/Sf9 expression system as previously described (Inoue et al., 2015) with the following titers; AAV2/1- pCaMKIIα-GCaMP6f-WPRE (1.0×10^{13} GC/ml), AAV2/1-pCaMKIIα-G-CaMP9a-WPRE (1.0×10^{13} GC/ml), AAV2/1-phSyn-Flpo (1.0×10^{13} GC/ml), AAV2/1-pCaMKIIα-iCre-T2A-EGFP-WPRE (3.0×10^{13} GC/ml), AAV2/1-pCAG-Flpo-T2A-TurboFP635-WPRE (3.0×10^{13} GC/ml), AAV2/1-pCAG-tTA-WPRE (3.0×10^{13} GC/ml), and AAV2/1-peSyn-XCaMP-R-WPRE (1.0×10^{13} GC/ml). Virus injections were performed on 4 weeks of age C57BL/6 wild-type or G-CaMP9a/R-CaMP2 transgenic mice. Each virus was stereotaxically injected into the barrel cortex (A/P −1.5 mm, M/L −2.7 mm from the bregma, D/V −0.3 mm from the pial surface) or visual cortex (A/P +0.3 mm, M/L −2.7 mm from the lambda, D/V −0.3 mm from the pial surface) under anesthesia. The viral solution was injected at 30 nl/min at a volume of 800 nl. After 4 weeks of expression, mice were subjected to *in vivo* two-photon calcium imaging or immunohistochemistry. We note that the time courses of G-CaMP9a induced by AAV2/1-phSyn-Flpo are the same as that induced by *in utero* electroporation.

Tissue preparation and immunohistochemistry

Tissue preparation and immunohistochemistry were performed as described previously with minor modifications (Sakamoto et al., 2014). Mice were deeply anesthetized with Chloral hydrate/xylazine and transcardially perfused with 25 ml of PBS and 50 ml of 4% PFA/PB (pH 7.4). Brains were postfixed in the perfusing solution overnight at 4°C and then immersed for 24 h in 30% sucrose in PBS. Brains were embedded in OCT compound and frozen at −80°C. Cryostat sections (30 μm thick) were incubated in 5% normal goat serum and 0.1% Triton X-100/PBS at room temperature for 1 h, incubated with primary antibodies diluted 0.1% Triton X-100/PBS containing 1% normal goat serum overnight at 4°C. The following primary antibodies (final dilution, source) were used: rabbit anti-GFP (1:1000, Thermo Fisher Scientific), rat anti-GFP (1:1000, 1:1000, Nacalai tesque), rabbit TurboFP635 (1:2000, Evrogen), rat anti-RFP (1:2000, Chromotek), rat anti-somatostatin (1:300, Millipore). The sections were washed with PBS and then incubated with secondary antibodies conjugated to Alexa-488 (1:500, Thermo Fisher Scientific), Alexa-594 (1:500, Thermo Fisher Scientific), and Hoechst 33422 (Thermo Fisher Scientific) for 1 h at room temperature. The sections were mounted with a clean mount (Electron Microscopy Science) and photographed with a confocal laser-scanning microscope (LSM 710, Carl Zeiss).

Animal surgery for *in vivo* imaging

Mice (1–5 months of age) of both sexes were anesthetized by isoflurane (3.0% v/v for induction, 1.5–2.0% during surgery). Before surgery, dexamethasone sodium phosphate (2 mg/kg-BW; Wako) and carprofen (5 mg/kg-BW; Zoetis) were administered intraperitoneally. During surgery, mice were put on a heating pad, and body temperature was kept at 37°C. A custom-made stainless steel head plate was fixed to the skull using cyanoacrylate adhesive and dental cement (Sun-medical) above the left visual cortex (centered 3.0 mm lateral to the midline and 0.5 mm anterior of lambda) or barrel cortex (centered 3.0 mm lateral to the midline and 1.5 mm posterior of bregma). Craniotomies were drilled with a 2.5 mm diameter, and the brain was kept moist with saline. A cover glass (3 mm diameter, Warner Instruments) was placed with surgical adhesive glue (Aron Alpha A, Sankyo). After the recovery, animals were transferred to the animal stage under the two-photon microscope.

In vivo calcium imaging

In vivo imaging was conducted with a two-photon microscope (LSM 710, Carl Zeiss) using a 20x/1.0 N.A. water immersion objective and tunable Ti: Sapphire laser (Chameleon Ultra II, Coherent). *In vivo* imaging of GECI-expressing neurons was performed in layer 2/3 of the left visual or barrel cortex (approximately 200–250 μm from the pia) or layer 5 of the barrel cortex (approximately 450–500 μm from the pia). The laser wavelength was tuned at 940 nm (G-CaMP9a) or 990 nm (G-CaMP9a/X-CaMP-R). To acquire GECI fluorescence, we used a 500–550 nm bandpass filter (G-CaMP9a) (Carl Zeiss) and a 575–650 nm bandpass filter (XCaMP-R) (Semrock). The laser power was between 54 and 213 mW at the front aperture of the objective. Spontaneous and sensory-evoked activities of neuronal populations were recorded at the resolution of 256 × 256 pixels (frame rate = 4 Hz). Fluorescence emissions were collected using a GaAsP photomultiplier tube (Hamamatsu photonics). During imaging, the head-fixed mice are awake and can walk on a circular treadmill.

High-speed *in vivo* imaging (Figure S3, Video S2) was conducted with a two-photon microscope (FVMPE-RS, Olympus) using a 25x/1.05 N.A. water immersion objective and tunable laser (Insight DS +Dual, Spectra-Physics). The laser wavelength was tuned at 940 nm. To acquire GECI fluorescence, we used a 495–540 nm bandpass filter (Olympus). Spontaneous activities were recorded at the resolution of 512 × 512 pixels (frame rate = 30 Hz). Fluorescence emissions were collected using a GaAsP photomultiplier tube (Hamamatsu photonics). During imaging, the head-fixed mice are awake and can walk on a circular treadmill.

Sensory stimulation

Visual stimulation was performed as described previously with minor modification (Ayzenshtat et al., 2016; Chen et al., 2013; Inoue et al., 2019). The moving grating stimuli were generated using MATLAB (Mathworks) and the Psychophysics Toolbox (Brainard, 1997). Each stimulus trial consisted of a 4 s blank period followed by a 4s drifting sinusoidal grating (0.05 cycles per degree, 1 Hz temporal frequency). Eight drifting gratings were used (separated by 45°), and 5 trials were recorded for each direction. The gratings were presented with an LCD monitor (19.5 inches, Dell), placed 25 cm in front of the center of the right eye of the mouse. Whisker stimulation was applied to contralateral whiskers using a brief air puff (50 ms) using a microinjector (BEX).

Image analysis

Images were analyzed with ImageJ (NIH) and MATLAB (Mathworks). Motion correction was performed by the Suite2P toolbox (https://github.com/cortex-lab/Suite2P) (Pachitariu et al., 2017) or the TurboReg plug-in in ImageJ (Thevenaz et al., 1998).

For *in vivo* calcium imaging in the visual cortex, a semi-automatic segmentation of regions of interest (ROIs) was then performed in the motion-corrected data using the Suite2P toolbox. $\Delta F/F_0$ was calculated as $(F - F_0)/F_0$, where the fluorescence intensity at any time points and F_0 is baseline fluorescence signal averaged over a 2-s period before starting the stimulation. Visual responses were measured for each trial as $\Delta F/F_0$, averaged over the stimulus period. Visually responsive neurons were defined using ANOVA across blank and eight direction periods ($p < 0.01$) (Ohki et al., 2005) with an average $\Delta F/F_0$ at preferred orientations greater than 6%. Of the responsive cells, orientation-selective neurons were defined by ANOVA across eight direction periods ($p < 0.01$).

The orientation selectivity index (OSI) was calculated for visually responsive cells (Chen et al., 2013; Niell and Stryker, 2008). First, the preferred orientation (θ_{pref}) of the cell was determined as the stimulus that produced the most robust response. The orientation tuning curve was constructed by measuring the mean $\Delta F/F_0$, averaged over the stimulus period, for each orientation. We then fitted the tuning curve with the sum of two Gaussians centered on θ_{pref} and $\theta_{pref} + \pi$, both with width σ (constrained to >15°), amplitudes A1 and A2, and a constant baseline B. The OSI was defined as $OSI = (R_{pref} - R_{ortho})/(R_{pref} + R_{ortho})$, where R_{pref} and R_{ortho} are the response amplitudes at the preferred (θ_{pref}) and the orthogonal orientation ($\theta_{pref} + \pi/2$) respectively.

For calcium imaging in the barrel cortex, $\Delta F/F_0$ was calculated as $(F - F_0)/F_0$, where F is the fluorescence intensity at any time point, and F_0 is the twentieth percentile of total fluorescence intensity. Decay time constants were measured through a single exponential fitting for every calcium transient exceeding 3 SD of the baseline fluctuation from peak response to baseline.

QUANTIFICATION AND STATISTICAL ANALYSIS

Statistical analyses of the acquired data were performed using MATLAB Statistics Toolbox (Figures 3 and 5) (Mathworks) and Prism 9 (Figures 1 and 4) (GraphPad). For each figure, a statistical test matching the structure of the experiment and the structure of the data was employed. $*p < 0.05$; $**p < 0.01$; $***p < 0.001$; n.s., not significant ($p > 0.05$) for all statistical analyses presented in figures. Experimental sample sizes are mentioned in the figure panel and legends.